Coastal Engineering 55 (2008) 1028–1040

Contents lists available at ScienceDirect

Coastal Engineering

journal homepage: www.elsevier.com/locate/coastaleng

Analysis of dune erosion processes in large-scale flume experiments

J.S.M. van Thiel de Vries [a,b,*], M.R.A. van Gent [b], D.J.R. Walstra [a,b], A.J.H.M. Reniers [a,c]

[a] Delft University of Technology, The Netherlands
[b] Delft Hydraulics, The Netherlands
[c] Rosentiel School, University of Miami, USA

ARTICLE INFO

Article history:
Received 20 July 2007
Received in revised form 13 March 2008
Accepted 3 April 2008
Available online 2 June 2008

Keywords:
Dune erosion
Large-scale physical model tests
Inner surf and swash zone
Infragravity waves
Wave breaking
Pressure gradients
Acceleration skewness

ABSTRACT

Large-scale physical model tests were conducted with different wave periods to examine the physical processes driving dune erosion. The model tests have been carried out in a flume (2DV) with a sandy dune exposed to extreme surge and wave conditions [Van Gent, M.R.A., Van Thiel de Vries, J.S.M., Coeveld, E.M., De Vroeg, J.H. and Van de Graaff, J., 2008. Large-scale dune erosion tests to study the effect of wave periods. Coastal Engineering. doi:10.1016/j.coastaleng.2008.04.003.]. Detailed measurements in time and space of water pressure, flow velocities and sediment concentrations were performed in the near shore area. The data revealed that both short- and long waves are important to inner surf hydrodynamics. Depth averaged flows are directed offshore and increase towards the shore line. The corresponding mean sediment concentrations rise sharply towards the dune face (up to 50 g/l near the bed). The strong increase in the mean sediment concentration towards the dune face correlates well with the maximum wave surface slope which in turn is coupled to both the pressure gradient and the near-bed wave-breaking induced turbulence. Analysis shows that the pressure gradient is only partially coupled to the flow acceleration suggesting that the latter cannot always be used as a proxy for the first. Weak correlation is obtained with the near-bed flows related to the bed shear stress. Tests with a larger wave period resulted in a larger dune erosion volume. During these tests more wave energy (combined incident and infragravity waves) reached the dune face, but more importantly, this wave energy is dissipated by fewer waves resulting in more intense wave breakers and steeper wave fronts. It is therefore expected that the wave-breaking induced near-bed turbulence increases resulting in significantly higher (O(100%)) mean sediment concentrations. In addition the mean flow velocities are comparable, yielding a substantially larger offshore directed sediment transport capacity. This increase in offshore directed transport is only partially compensated by a concurrent increase in the wave related onshore transport capacity associated with intrawave processes, resulting in a net increase in the dune erosion rate.

1. Introduction

Large parts of the Netherlands are situated below mean sea level and are prevented from flooding by a narrow strip of sandy beaches and dunes. Since economic hinterland values are large and the area is densely populated the Dutch government assesses the strength of dunes against normative storm conditions every five years. This assessment is performed with an empirical guideline based on dune erosion experiments in a flume (Vellinga, 1986). Recent analyses of the wave climate along the Dutch coast have revealed that the peak wave period for the normative storm conditions is expected to be significantly higher than anticipated in the past (De Ronde et al., 1995; Roskam and Hoekema, 1996). These wave periods are not covered by the previous flume experiments. Hence, new large-scale dune erosion experiments were required to assess the effect of wave periods on dune erosion during extreme storm conditions. It was found that increasing the wave period with 50% from T_p=12 s to T_p=18 s results in 24% more dune erosion (Van Gent et al., 2008).

Given the fact that the empirical guidelines are based on a limited set of experiments they are not generic. For instance they do not take into account the non-uniformity of a coast in alongshore direction. At several locations sandy coasts are expected to behave as a three dimensional system due to strong curvature of the coast line, the alternation of soft dunes with hard elements or a strongly variable fore shore in the alongshore direction. To assess the strength of dunes in these complex coastal systems a more advanced guideline is required which can be based upon a process based model instead, provided the model includes all the relevant physical processes for dune erosion under extreme storm conditions.

At the moment our understanding of the dune erosion processes is inadequate in both cross shore and alongshore direction, especially close to the dune front, for a successful model implementation. Therefore, the objective of the present paper is to study detailed

* Corresponding author. P.O. Box 5048, 2600 GA Delft, The Netherlands. Fax: +31 15 2785124.
E-mail address: j.s.m.vanthieldevries@tudelft.nl (J.S.M. van Thiel de Vries).

0378-3839/$ – see front matter © 2008 Elsevier B.V. All rights reserved.
doi:10.1016/j.coastaleng.2008.04.004

Table 1
Test program

Test	Interval	H_{m0} [m]	T_p [s]	$T_{m-1,0}$ [s]	SWL [m]	Spectrum shape	Remark
T01	A–E	1.50	4.90	4.45	4.50	Pierson–Moskowitz	Repeated
	F	1.50	4.90	4.45	4.50	Pierson–Moskowitz	
	G	1.50	7.35	6.68	4.50	Pierson–Moskowitz	
	H	0.50	7.35	6.68	4.50	Pierson–Moskowitz	
	I	1.40	5.00	4.54	4.50	Pierson–Moskowitz	
T02	A–E	1.50	6.12	5.56	4.50	Pierson–Moskowitz	
T03	A–E	1.50	7.35	6.68	4.50	Pierson–Moskowitz	Repeated
	F	0.80	7.35	6.68	4.50	Pierson–Moskowitz	
T04	A–E	1.50	7.35	6.68	4.50	Pierson–Moskowitz	
DP01	A–E	1.50	6.12	3.91	4.50	Double peaked	
	F	0.50	7.35	6.68	4.50	Pierson–Moskowitz	
DP02	C–E	1.50	7.35	5.61	4.50	Double peaked	

measurements obtained during a large-scale dune erosion experiment in order to obtain more insight in the cross shore processes important to dune erosion. To this end wave characteristics over the fore shore, near shore hydrodynamics, sediment concentrations and transports are studied.

Large-scale experiments to examine dune erosion have been performed in the past (Dette, 1986; Vellinga, 1986; Kraus and Smith, 1994; Roelvink and Reniers, 1995; Dette et al., 2002) however the instrument deployment was generally restricted to the surf zone and wave periods did not cover the range of interest. The present set of experiments focuses on extreme storm conditions (return period of 10,000 years) and instrument deployment is in close proximity of the dune face to examine the dune erosion processes.

The paper first addresses the instrument deployment and briefly discusses the physical model setup. Next in-situ measurement results are analyzed and discussed to gain insight in the physical processes important to dune erosion at the short wave, infragravity and mean time scales. This is followed by an analysis of the effect of a larger wave period on dune erosion and near dune physics. The paper ends with discussion and conclusions.

2. Instrument deployment and physical model description

Six large-scale dune erosion experiments were conducted in the Delft Hydraulics Delta flume from November 2005 through February 2006. The hydrodynamic boundary conditions for each test varied and are listed in Table 1. The initial profile for all tests is shown in Fig. 1 and the diameter of the applied sediment was D_{50}=200 μm. Duration of a test was at least 6 h and tests were divided into intervals (A–E). After each interval the tests were interrupted at 0.10, 0.30, 1.00, 2.04 and 6.00 h to carry out profile measurements along three transects in the flume. A first profile measurement was conducted along the longitudinal flume axis and the other two at 1.25 m on either side of this axis.

Tests T01 and T03 were repeated to check consistency and in tests T01, T03 and DP01 additional experiments were performed as listed in Table 1. Between additional intervals also profile measurements were carried out. A more extensive description of the physical model setup and the bed profile measurements is found in Delft Hydraulics (2006) and in Van Gent et al. (2008).

In-situ measurements were obtained in two clusters that were deployed respectively on the flume wall, and a mobile frame. In addition two camera pairs were installed to obtain stereo video data with the objective to make three dimensional reconstructions of dune face and near shore (Van Thiel de Vries et al., 2007). This paper describes and analyses the in-situ measurement series.

2.1. Instruments deployed on flume wall

Ten pressure sensors were spaced along the flume wall to measure wave transformation over the fore shore (Fig. 1 and Table 2). A collocated pressure- and electromagnetic current velocity sensor and three vertical resistance wires were installed centered around x=41 m to distinguish between incoming and shore line reflected waves. Two electromagnetic current velocity sensors were deployed at x=200 m and x=205 m to measure near shore hydrodynamics. All devices on the flume wall were synchronized and sampled with 20 or 25 Hz depending on the specific test. At the beginning of a test electromagnetic current velocity- and pressure sensor output voltages were set to zero in still water to obtain information about wave setup and time-averaged flow.

2.2. Instruments deployed on mobile frame

A frame was fixed to a mobile carriage to measure water pressure and the vertical structure of the flow- and sediment concentrations at several cross shore positions in the flume. Vertical positioning of the mobile frame was realized by telescoping steel pipes controlled by a winch (Fig. 2). The weight of the frame was guided to the sand bed by a fork shaped steel construction and an instrument pipe was placed between the steel fork legs. All mobile frame devices were deployed on the instrument pipe which could move vertically independent from the rest of the construction using a second winch. The detailed vertical positioning of the instruments was known in relation to the local bed by lowering the instrument pipe till a small steel plate rested on the bed. If this plate stood on the bed the instrument pipe winch was tightened again to prevent settling and to keep device elevations constant in relation to the bed. The vertical positioning system does not adjust to bed level changes that are presumed to be minimal within a mobile frame measurement.

The mobile frame was deployed during tests T04, DP01, DP02 and the repetition of test T01 and T03. Measurements have a typical length of 10 to 20 min after which the frame was positioned at another cross

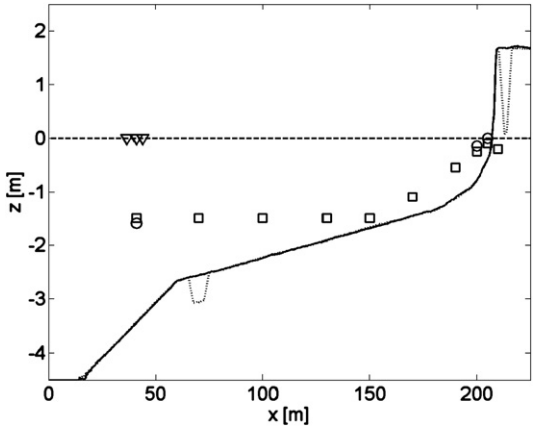

Fig. 1. Initial profiles for all tests (solid line) except T04 (dotted line) and deployed instruments on the flume wall (markers) during the Delta-flume experiment. The still water level is shown by the dashed line. The wave board is at the origin of the coordinate system (x=0); y=0 is at the middle of the flume and z=0 coincides with still water level. Devices on the flume wall consist of ten pressure sensors (squares), three electromagnetic current velocity sensors (circles) and three resistance wires (triangles).

Table 2
Vertical position of instruments installed on flume wall in relation to flume bottom

	PS01	PS02	PS03	PS04	PS05	PS06	PS07	PS08	PS09	PS10	EMF01	EMF02	EMF03
x [m]	41	70	100	130	150	170	190	200	205	210	41	200	205
z [m]	−1.50	−1.50	−1.10	−1.10	−1.10	−1.10	−0.55	−0.35	−0.20	−0.25	−1.60	−0.15	0.00

shore location. Wave properties were measured with a pressure sensor and the vertical structure of the flow was obtained with eight electromagnetic current velocity sensors (EMF's) (Table 3). The pressure sensor and four EMF's positioned closest to the bed were synchronized with devices on the flume wall and sampled with 20 Hz or 25 Hz depending on the specific test. The upper four EMF's had a 2 Hz sample rate and are only used to measure time-averaged flow.

Time-averaged sediment concentrations were measured with ten suction tubes vertically spaced along the instrument pipe and directed normal to the plane of orbital motions (Bosman et al., 1987). Instantaneous sediment transports were measured with four optical backscatter sensors (OBS's), an acoustic sediment transport meter (ASTM) and an ultrasonic high concentration meter (UHCM) (Fig. 2 and Table 3). The OBS's (transmitting infrared beam) and UHCM (transmitting 5 MHz signal) were synchronized with devices on the flume wall and had a 20 Hz sample frequency. The ASTM transmits a 4.4 MHz signal (in order to minimize grain size dependency) and samples with 2 Hz. Sediment concentration devices were installed at the same vertical elevation from the bed as EMF's as much as possible (Table 3). Instrument configuration of the mobile frame during test DP01, T04, and repetition of T01 and T03 deviated from

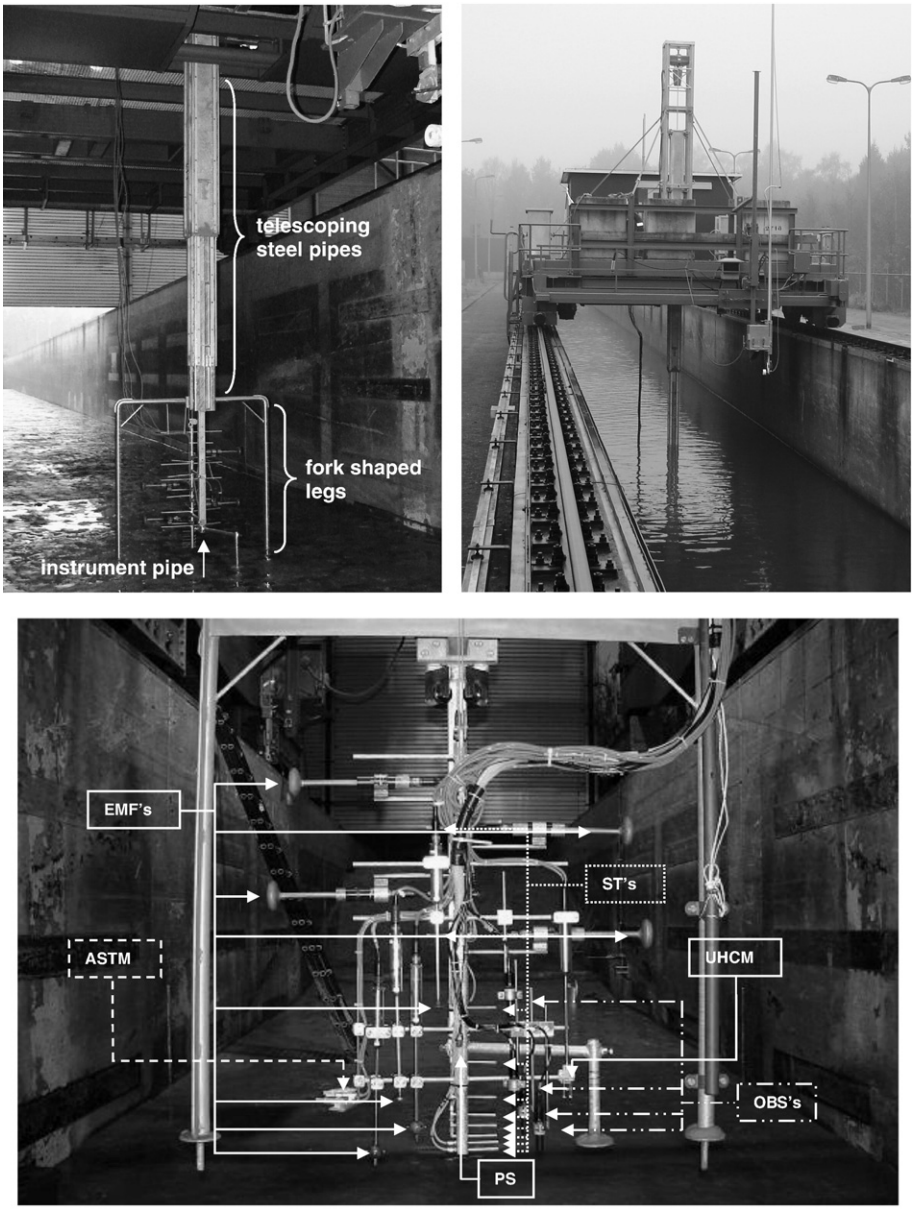

Fig. 2. Overview mobile frame. Upper left image: the mobile frame in an empty flume. Upper right image: shallow water frame in production. Lower image: close-up of the devices installed on the instrument pipe.

Table 3
Vertical position of instruments installed on mobile frame in relation to local bed

z_b [m]	ST	EMF	OBS	UHCM	ASTM	PS
0.04	ST01					
0.06	ST02	EMF07	OBS02			
0.08	ST03					
0.11	ST04	EMF06	OBS01			
0.14	ST05					
0.19	ST06	EMF05	OBS04	UHCM	ASTM	PS11
0.29	ST07					
0.44	ST08	EMF04	OBS03			
0.64	ST09	EMF10				
0.74		EMF11				
0.94	ST10	EMF09				
1.07		EMF08				

that in Table 3. More information about instrument configuration during these tests is found in Delft Hydraulics (2006).

3. Test results

For brevity this section only discusses measurements from test T01. In Section 4 measurements from test T01 and T03 are compared to examine the effect of the wave period on dune erosion.

3.1. Waves

Near dune pressure sensors were installed in shallow water close to the bed and rarely came out of the water. Time series from pressure sensors spaced along the flume wall and deployed on the mobile frame are translated into water surface elevations using linear wave theory. Wave height transformation over the fore shore of short- and long waves is obtained from water surface variance in wave frequencies respectively higher- and lower than half the deep water peak frequency ($f_{split}=0.5\,f_p$). The wave setup (η_m) is computed from the pressure sensors on the flume wall as the average water surface elevation in relation to still water level.

Wave transformation over the fore shore during test T01 is shown in Fig. 3, upper left panel. Waves start to break immediately after generation near the wave board (visual observation) and as a result a section with shoaling waves is not observed in the flume. In landward direction short wave height decreases whereas the long waves gain slightly more height. Close to the dune face the long wave energy exceeds that of short waves. The spectral mean wave period $T_{m-1,0}$ increases in direction of the shore (Fig. 3, lower left panel) from 5.4 s at $x=41$ m to 26.8 s at $x=205$ m consistent with a shift of wave variance towards lower frequencies. With progress of a test the fore shore develops and the total wave height near the shore at $x=205$ m decreases from 0.52 m in interval A to 0.35 m in interval E, a reduction of more than 30%. This is caused by a decline of both short- and long wave heights (Fig. 3, upper right panel). Note that the relative importance of long wave energy near the dune face increases as a test continues (Fig. 3, upper- and lower right panels).

Observations during the experiment also revealed that waves reflect near the shore line. This is illustrated in Fig. 4 left panel that shows the normalized correlation between flow velocity- and water surface elevation time series for the mobile frame measurements

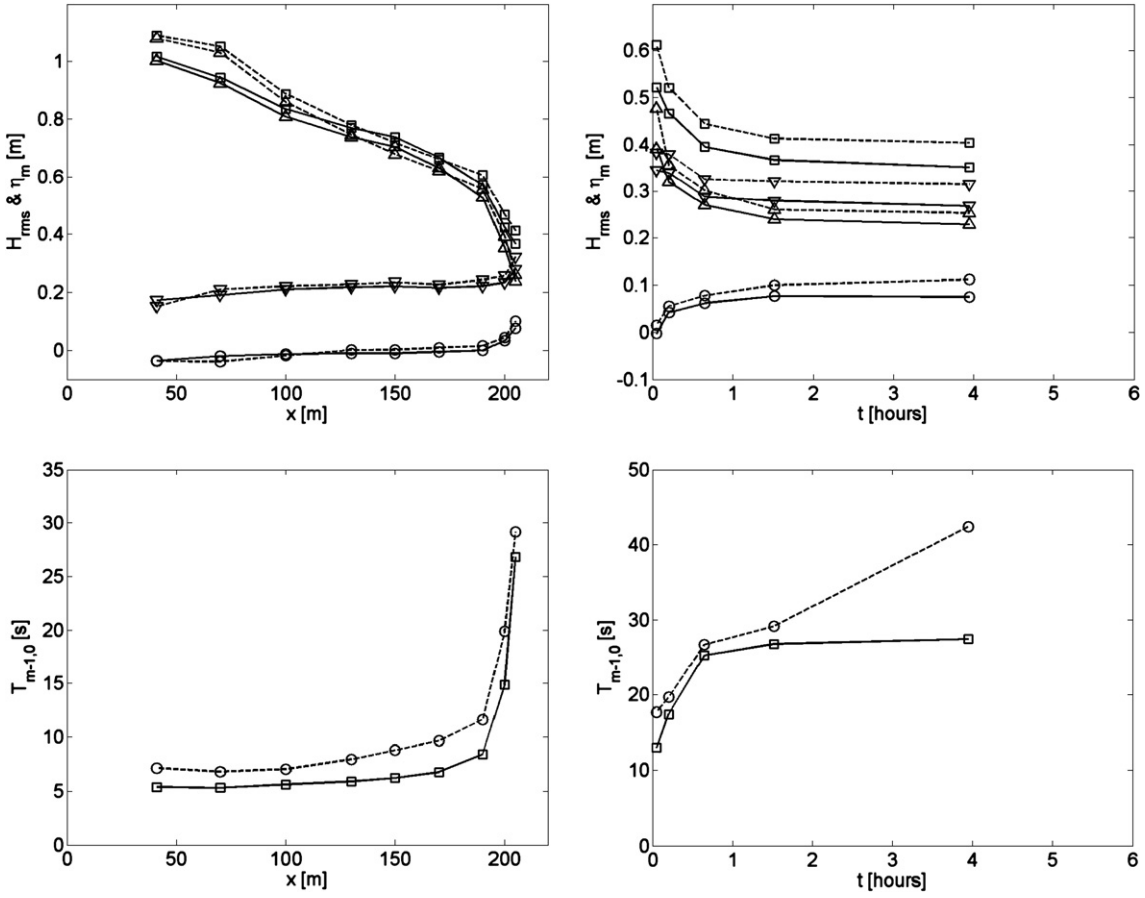

Fig. 3. Upper left panel: transformation of total wave height (squares), short wave height (upward pointing triangles), long wave height (downward pointing triangles) and wave setup (circles) as function of the cross shore distance for test T01 (solid line) and test T03 (dashed line). Upper right panel: temporal evolution of wave heights and setup for test T01 (solid line) and test T03 (dashed line) at $x=205$ [m]. Lower left panel: spectral mean wave period as function of cross shore distance for test T01 (solid line–squares) and test T03 (dashed line–circles). Lower right panel: temporal evolution of spectral mean wave period for test T01 (solid line–squares) and test T03 (dashed line–circles).

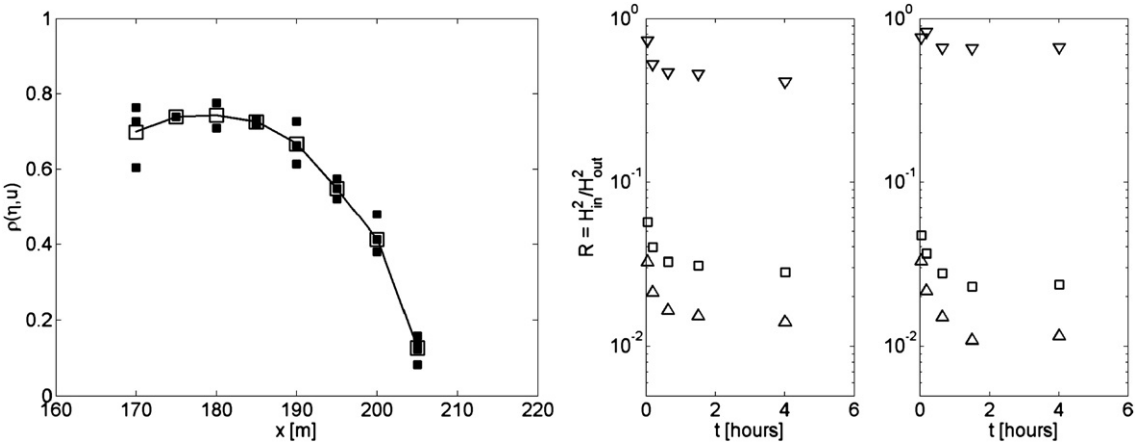

Fig. 4. Left panel: correlation ρ between water surface elevation $\eta(t)$ and flow velocity $u(t)$ as a function of cross shore position. Right panel: wave energy reflection coefficients for all waves (squares), short waves (upward pointing triangles) and long waves (downward pointing triangles) during test T01 (left) and T03 (right).

during test T01. Considering progressive waves we expect a correlation close to one whereas for a standing wave pattern the correlation should be close to zero. It is shown that in the near dune area ($x \geq 170$) the correlation between $u(t)$ and $\eta(t)$ decreases rapidly from about 0.75 at $x=170$ m till 0.15 at $x=205$ m. A partly standing wave pattern is present in the near dune area.

In order to further examine this partly standing wave pattern the collocated pressure and current velocity sensor at $x=41$ m are used to decompose the measured water surface elevations in incoming- and shoreline reflected short- and long wave heights. For this purpose we use a method presented by Guza et al. (1984):

$$\eta_{\text{in}} = \frac{\eta c_{\text{out}} + Q}{c_{\text{in}} + c_{\text{out}}} \text{ and } \eta_{\text{out}} = \frac{\eta c_{\text{out}} - Q}{c_{\text{in}} + c_{\text{out}}} \tag{1}$$

where η_{in} and η_{out} are the water surface elevations associated with respectively the incoming and shore line reflected waves. $Q=uh$ in which u is the depth averaged flow estimated using linear wave theory and h is water depth. In contrast with Guza the decomposition is performed in Fourier space. Also c_{in} and c_{out}, respectively the wave celerities of the incoming and reflected waves, are computed differently. It is assumed that all frequencies propagate with their free velocity except for the incoming wave frequencies smaller than f_{split}, which are considered as bound long waves that propagate with the wave group velocity c_{g}, associated with the $T_{m-1,0}$ wave period:

$$c_{\text{in}} = \begin{cases} c_{\text{in},1} = \omega/k & , f \geq f_{\text{split}} \\ c_{\text{in},2} = c_{\text{g}} & , f < f_{\text{split}} \end{cases} \quad c_{\text{out}} = \omega/k$$

where $\omega=2\pi f$ and f is the wave frequency. It was found that for the sensor at $x=41$ m $c_{\text{g}} \approx \sqrt{gh}$.

Short wave reflections are found to be small ($E_{hf,\text{out}} / E_{hf,\text{in}} < 3\%$) and decrease with progress of a test (Fig. 4, Right panel). Reflected long wave energy is significantly larger (initially $E_{lf,\text{out}} / E_{lf,\text{in}} = 75\%$) and decreases till 40% in interval E. Considering all waves, reflected wave energy is less than 5% at $x=41$ m.

3.2. Flow

Mobile frame flow velocity measurements were obtained in the near shore area over the developing fore shore in order to obtain more insight in the time and depth averaged return flow, the time-averaged near-bed flow and the importance of short- versus long wave orbital motions. Depending on the mobile frame location velocity sensors could be temporally above the water surface. Since electromagnetic current velocity sensors above the water surface drift to a random value, only time series from flow sensors placed below the wave trough are analyzed. The wave trough is defined as $\eta_{\text{tr}} = <\eta_{\text{min}}>$, where η_{min} is the minimum water surface elevation in a zero crossing wave and $<>$ means taking the average. Flow velocity time series obtained below wave trough may contain spikes due to turbulence and air inclusion, especially in areas with intense wave breaking. Spikes with amplitude larger than 0.25 m/s and duration smaller than 1.0 s are removed and replaced by linearly interpolated values. In order to measure time-averaged flows, flow velocity sensors were calibrated in still water. During test T03 this calibration took place in shallow water which is not preferable since, due to the proximity of the bottom and water surface, the calibration might cause an artificial offset to the flow devices. It was found that EMF06 had such an offset. As a consequence time-averaged flow velocities from EMF06 during test T03 are not included in the further analysis.

Time-averaged flow velocities which are of interest to the morphological response of a sandy dune system are considered to be both the near bottom- and depth averaged flow velocities. The near bottom flow is related to the shear stress exerted on the bed and in addition to bed load and the amount of sediment brought into suspension. The depth averaged velocity (below the wave trough) is usually related to advection of suspended sediment in 2DH models. Time-averaged near-bed flows are obtained from time series of the flow velocity sensor closest to (6 cm above) the bed. Depth averaged flows are obtained by vertical integration of measured mean flow velocities below the wave trough (Reniers et al., 2004b):

$$u_{mm} = \frac{1}{h}\int_{z=-h_0}^{z=\eta_{\text{tr}}} u_m(z)\mathrm{d}z \approx \frac{1}{h_0 + z_N}\sum_{j=1}^{j=N}\left(u_{\text{m},j} + u_{\text{m},j-1}\right)\left(z_j + z_{j-1}\right)/2 \tag{2}$$

where u_{mm} is the depth- and time-averaged flow velocity, h_0 is the still water depth, z_N is the vertical position of the first sensor below the wave trough, $u_{m,j}$ is the measured time-averaged flow velocity from a sensor located at vertical position z_j and $u_{m,j-1}$ and z_{j-1}, correspond to the first flow sensor installed below z_j. At the bed the flow velocity is assumed to be zero.

Near-bed flow velocities exceed depth averaged flow velocities within the cross shore range of mobile frame measurements (Fig. 5, upper left panel). Both the magnitude of near-bed- and depth averaged velocities increase gradually in shore ward direction till approximately $x=200$ m and drop drastically at $x=205$ m. Flow velocities at $x=205$ m should be interpreted with care since the number of flow velocity sensors below wave trough at this location is usually just one and vertical flow velocity gradients might be large. With progress of a test near-bed- and depth averaged flow velocities evolve differently depending on the cross shore location- and evolution (Fig. 5, upper right panel). Close to the dune face at $x=200$ m time-averaged flow velocities decrease 24% between the

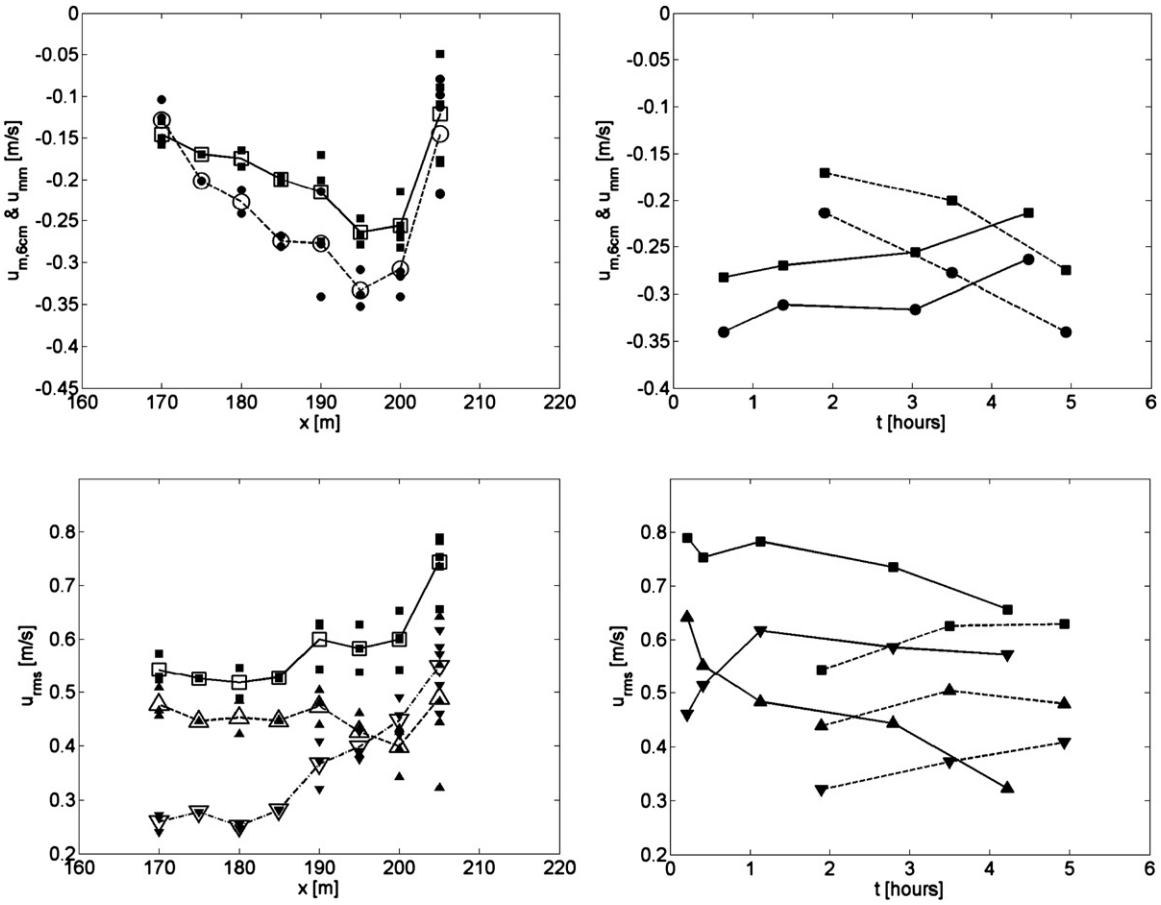

Fig. 5. Upper left panel: depth- and time-averaged flow velocities (squares) and time-averaged flow velocities 6 cm above the bed (circles) for test T01. Open markers are the average of all mobile frame measurements at a location within a test. Upper right panel: temporal evolution of depth- and time-averaged flow velocity (squares) and time-averaged flow velocity at 6 cm above the bed (circles) for test T01 at x=200 [m] (solid lines) and x=190 [m] (dashed lines). Lower left panel: transformation of total orbital velocities (squares), short wave orbital velocities (upward pointing triangles) and long wave orbital velocities (downward pointing triangles) over cross shore profile for test T01. Open markers are the average of all mobile frame measurements at a location within a test. Lower right panel: temporal evolution of total orbital velocities (squares), short wave orbital velocities (upward pointing triangles) and long wave orbital velocities (downward pointing triangles) for test T01 at x=205 [m] (solid lines) and x=190 [m] (dashed lines).

first and last measurement at this location whereas further seaward at x=190 m the average flow increases with 61%.

The presence of waves affects suspended sediment concentrations since near-bed orbital motions stir up sediment. In addition phase lags between the wave orbital flow and sediment suspension may directly contribute to sediment advection. Orbital flow velocities are computed as the standard deviation of near-bed velocity time series obtained at 6 cm above the bed. Similar to the wave heights, orbital velocities are split in a short- and long wave related part. Orbital velocities increase in shore ward direction from 0.6 m/s at x=170 m to about 0.8 m/s at x=205 m (Fig. 5, lower left panel). This increase can be attributed to a significant increase in long wave orbital velocities (from 0.25 m/s at x=170 m to 0.54 m/s at x=205 m) whereas short wave orbital velocities remain quite constant with decreasing water depth (0.51 m/s at x=170 m and 0.52 m/s at x=205 m). Close to the shore line at x=205 m long wave orbital velocities have the same order of magnitude as the short wave orbital velocities. The temporal evolution of orbital velocities varies with the cross shore position- and evolution (Fig. 5, lower right panel). Close to the dune face at x=205 m orbital velocities decrease 15% between the first and last measurement at this location. At the start of the test short wave orbital velocities exceed that of long waves whereas after 1 h the opposite is observed. Further offshore at x=190 m a 16% increase in orbital velocities is observed and short wave orbital velocities exceed that of long waves during the whole test.

3.3. Sediment concentrations

Time-averaged- and instantaneous sediment concentrations have been measured with the mobile frame over the developing fore shore. Time-averaged sediment concentrations obtained with suction tubes give robust results also between wave trough and top where tubes are regularly above the water surface. Output voltages from the instantaneous sediment concentration devices are calibrated with suction tube measurements. Time-averaged voltages from the OBS's and ASTM are correlated to time-averaged sediment concentrations obtained with suction tubes at the same height through which a second order polynomial is least square fitted (the correlation coefficients for respectively OBS1, OBS2, OBS3, OBS4 and the ASTM are 0.96, 0.93, 0.90, 0.96 and 0.39. The small correlation coefficient of the ASTM is caused by the limited measurement range of this instrument (up to 10 g/l)). A similar procedure is followed for the UHCM except that a first order polynomial is used (correlation coefficient is 0.95). More details about the calibration of the instantaneous sediment concentration devices are found in Delft Hydraulics (2006). In the ongoing analysis only time series from the OBS's are considered. Sediment concentration time series obtained above the wave trough (η_{tr}=<η_{min}>) are eliminated from analysis since OBS's that are regularly above the water surface give unrealistic peaks in sediment concentrations not corresponding to measurements obtained with OBS's installed below wave trough.

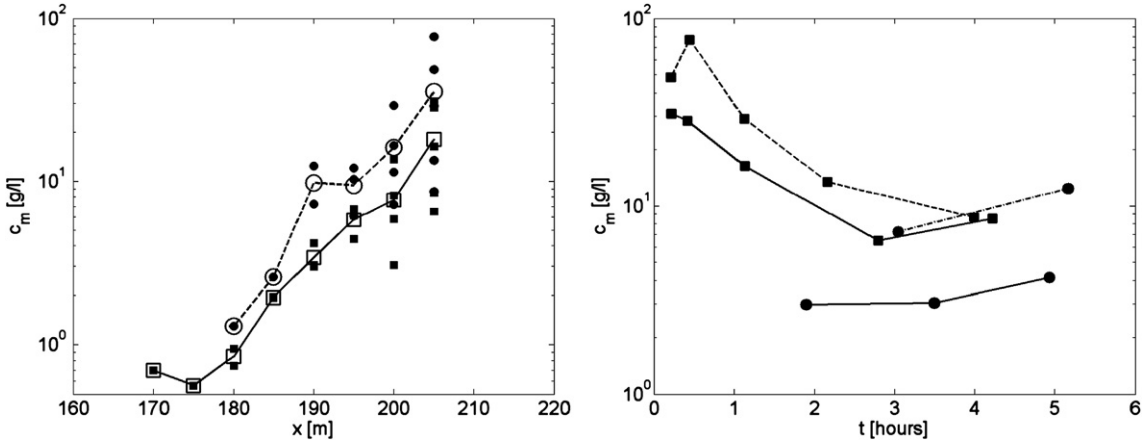

Fig. 6. Left panel: time-averaged sediment concentrations 6 cm above the bed as function of cross shore distance for test T01 (squares) and test T03 (circles). Open markers are the average of all mobile frame measurements at a location within a test. Right panel: temporal evolution of sediment concentrations for test T01 (solid lines) and test T03 (dashed lines) at x=205 [m] (squares) and x=190 [m] (circles).

Near-bed time-averaged sediment concentrations obtained with the suction tube located closest to (4 cm above) the bed increase with decreasing water depth from concentrations smaller than 1 g/l at x=180 m till up to more than 50 g/l at x=205 m (Fig. 6, left panel). With progress of a test the sediment concentrations close to the dune face (x=205 and x=200 m) decrease with more than 70% between the first and last measurement at this location whereas further offshore (x=190 m) sediment concentrations increase with 39% (Fig. 6, right panel). It was found that the standard deviation of instantaneous sediment concentration time series is positively related to the time-averaged sediment concentration (not shown).

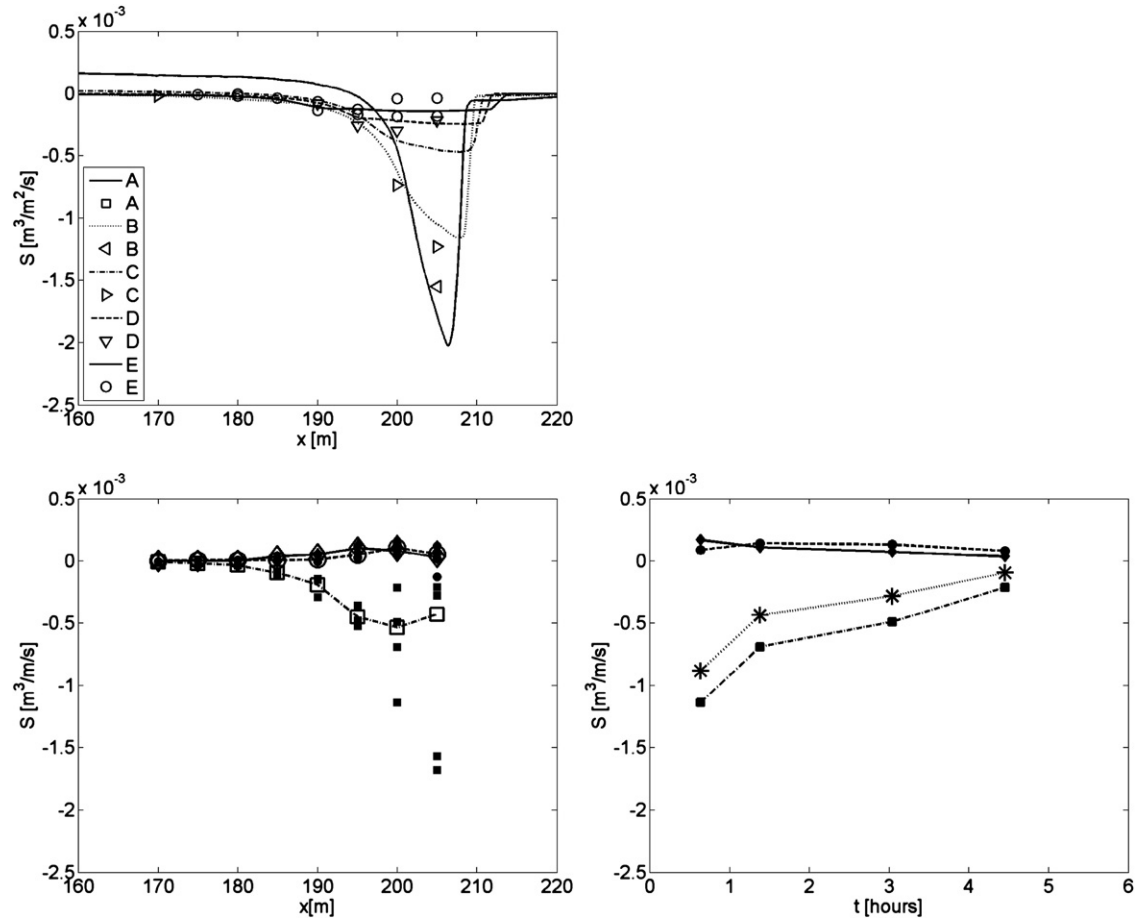

Fig. 7. Upper panel: sediment transports from bed level changes (lines) and mobile frame measurements (markers) at different intervals (see legend) as function of cross shore position for test T01. Lower left panel: mobile frame sediment transports split into flow related sediment transport (dashed-dotted line–squares), wave related sediment transport (dashed line–circles) and sediment transports above the wave trough (solid line–diamonds). Open markers are the average of all mobile frame measurements at a location within a test. Lower right panel: temporal evolution of flow related sediment transport (dashed-dotted line–squares), wave related sediment transport (dashed line–circles), sediment transport above the wave trough (solid line–diamonds) and the total sediment transport (dotted line–asterisks) at x=200 m.

3.4. Sediment transports

In sandy coastal systems the sediment transport is commonly split into bed load and suspended load (Fredsoe and Deigaard, 1992). Considering dune erosion the suspended load is dominant (Vellinga, 1986). Here, the total time and depth integrated sediment transport is estimated from profile evolution whereas the time and depth integrated suspended load is computed from flow- and sediment concentration measurements. The bed load cannot be estimated (accurately) from available measurements but is expected to be of minor importance.

The total sediment transports are computed from cross shore integration of bed level changes starting at the (dry) end of the flume (225 m from the wave board) where the sediment transport is known to be zero:

$$S_x(x) = \int_{x=225}^{x=x} \frac{\partial z}{\partial t}(1 - n_p)\mathrm{d}x \tag{3}$$

where S_x is the cross shore sediment transport, $\partial z / \partial t$ is the cross flume averaged bed level change between successive profile measurements and n_p is porosity. The sediment balance is artificially closed by redistributing the residual transport at the wave paddle uniformly over the sedimentation area. It is noted that a curvature in the cross flume bathymetry was observed after the experiments between x=60 and x=200 m (Delft Hydraulics, 2006). The differences in bed level in cross flume direction can be up to 0.1 m. In the present analysis bed level changes from the three transects are simply averaged which might lead to less accurate computed sediment transports from profile measurements.

Suspended sediment transports from flow- and sediment concentration measurements are computed summing three transport components. Two represent sediment transports below wave trough and consist of respectively time-averaged (flow related)- and instantaneous (wave related) sediment transports:

$$\begin{aligned} S_{x_1} &= \int_{z=-h}^{z=\eta_{tr}} c_m u_m \mathrm{d}z \\ S_{x_2} &= \int_{z=-h}^{z=\eta_{tr}} \overline{c_f u_f}\,\mathrm{d}z \end{aligned} \tag{4}$$

where c_m and u_m are the time-averaged part and c_f and u_f are the demeaned sediment concentration- and flow time series. The third component is an estimation of the sediment transport above the wave trough. Especially close to the dune face, sediment transports above the wave trough cannot assume to be close to zero since measured sediment concentrations are significant up till the water surface. Sediment transports above the wave trough are estimated by the product of depth averaged flow and mean sediment concentrations above the wave trough:

$$S_{x_3} = -u_{mm}(h + \eta_{tr})c_{mm}. \tag{5}$$

In this expression $-u_{mm}(h+\eta_{tr})$ represents the time-averaged discharge between wave trough and top obtained from continuity over the vertical and c_{mm} is the depth and time-averaged sediment concentration obtained with suction tubes between wave trough and top.

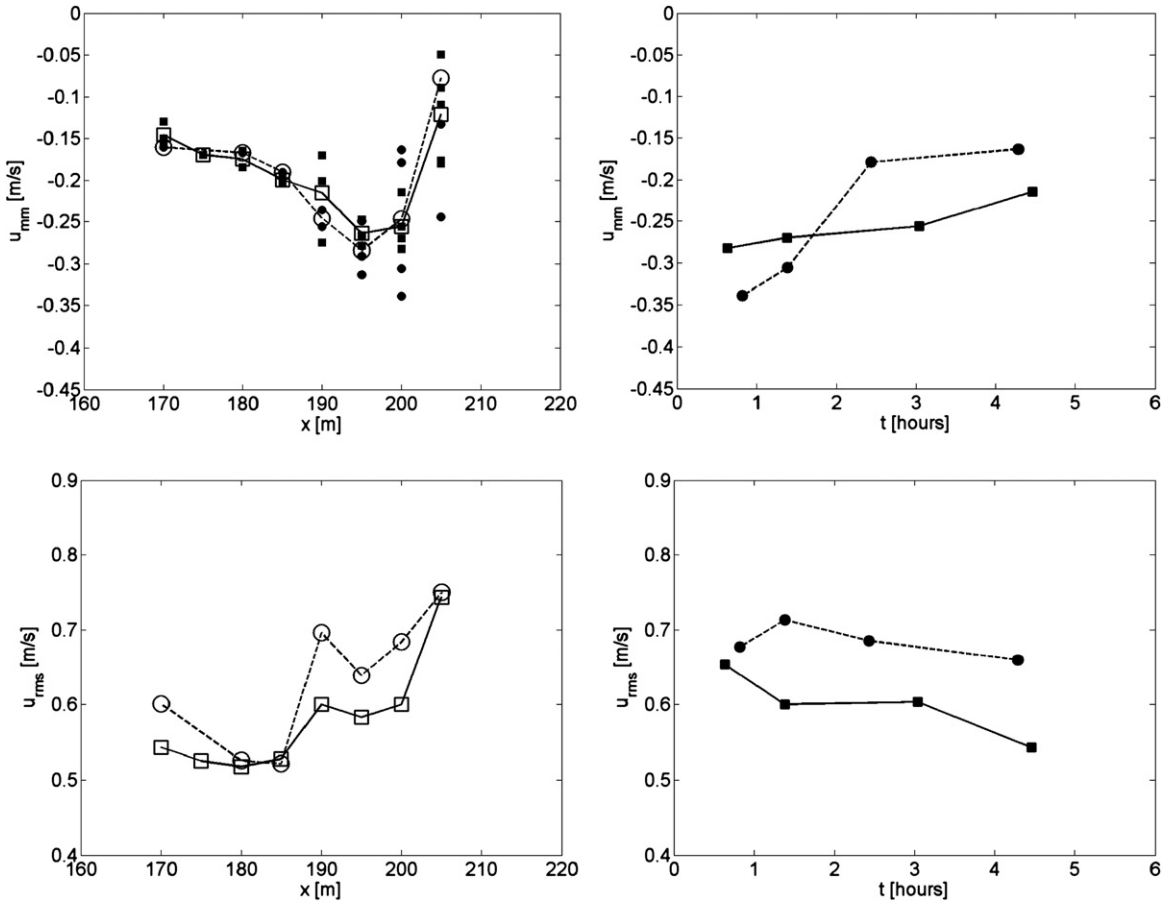

Fig. 8. Upper left panel: depth and time-averaged flow as function of cross shore distance for test T01 (solid line–squares) and test T03 (dashed line–circles). Open markers are the average of all mobile frame measurements at a location within a test. Upper right panel: temporal evolution of time and depth averaged flow for test T01 (solid line–squares) and test T03 (dashed line–circles) at x=200 [m]. Lower left panel: total orbital velocities as function of cross shore distance for test T01 (solid line–squares) and test T03 (dashed line–circles). Shown markers are the average of all mobile frame measurements at a location within a test. Lower right panel: temporal evolution of total orbital velocities for test T01 (solid line–squares) and test T03 (dashed line–circles) at x=200 [m].

Measured sediment transports from profile- and mobile frame measurements are shown in Fig. 7, upper left panel. Sediment transport magnitude increases in shore ward direction till the dune face where sediment transport gradients must reverse (erosion). As a test continues the near dune maximum sediment transport decreases with 95% between interval A and E. Temporal transport gradients are largest near the dune face and decay in offshore direction. The location of the maximum sediment transport, which is the transition of sedimentation and erosion, moves shore ward with dune face retreat. The sediment transport is dominated by the mean offshore directed flow whereas the onshore sediment transports are relatively small. In general the suspended sediment transports computed from flow and sediment concentrations exceed the total transports obtained from profile evolution. This can be explained if a significant onshore bed load transport is present; however uncertainties in the estimated total and suspended load might be significant and prevent any firm conclusions about magnitude and direction of the bed load.

4. Effect of a larger wave period on near shore processes

A 50% larger wave period during test T03 results in 24% more dune erosion after 2 h and 15% more erosion after 6 h (Van Gent et al., 2008). The objective is to improve our physical understanding of these effects by examining changes in wave transformation, flow, sediment concentrations and resulting transports for conditions with a larger wave period.

Wave transformation over the fore shore changes with an increase of the wave period (Fig. 3, upper left panel). Waves with on average a larger wave period initially loose less energy in the first 100 m of the flume. Between $x=120$ m and $x=160$ m wave heights are smaller in comparison to test T01 whereas close to the dune face ($x>190$ m) wave heights are larger again. Since near shore wave heights during test T03 exceed that of test T01 during the whole test with 10 to 15% (Fig. 3, upper right panel) it follows that for a larger wave period more energy reaches the dune face. The ratio between short wave and long wave variance remains the same with increasing wave period.

Time and depth averaged flow velocities have the same order of magnitude during test T01 and T03 (Fig. 8, upper left panel). The evolution of the depth averaged flow with progress of a test is different (Fig. 8, upper right panel). Initially the magnitude of the depth averaged flow at $x=200$ m in test T03 is larger. However, after approximately 2 h return flows during test T01 appear to be stronger. It is remarked that the overall observed larger near dune wave heights ($x>200$ m) during test T03 do not result in a larger return flow. This could be related to the increased setup level close to the shore (see Fig. 3), however the sparse instrument coverage at these locations prevents any firm conclusions.

Orbital flow velocities in test T03 at locations shoreward of $x=185$ m are larger in relation to test T01 (Fig. 8, lower left panel). At $x=205$ m the magnitude of orbital flows are comparable. Considering the temporal evolution of orbital velocities, no clear trend was observed comparing both tests at $x=205$ m. However results at

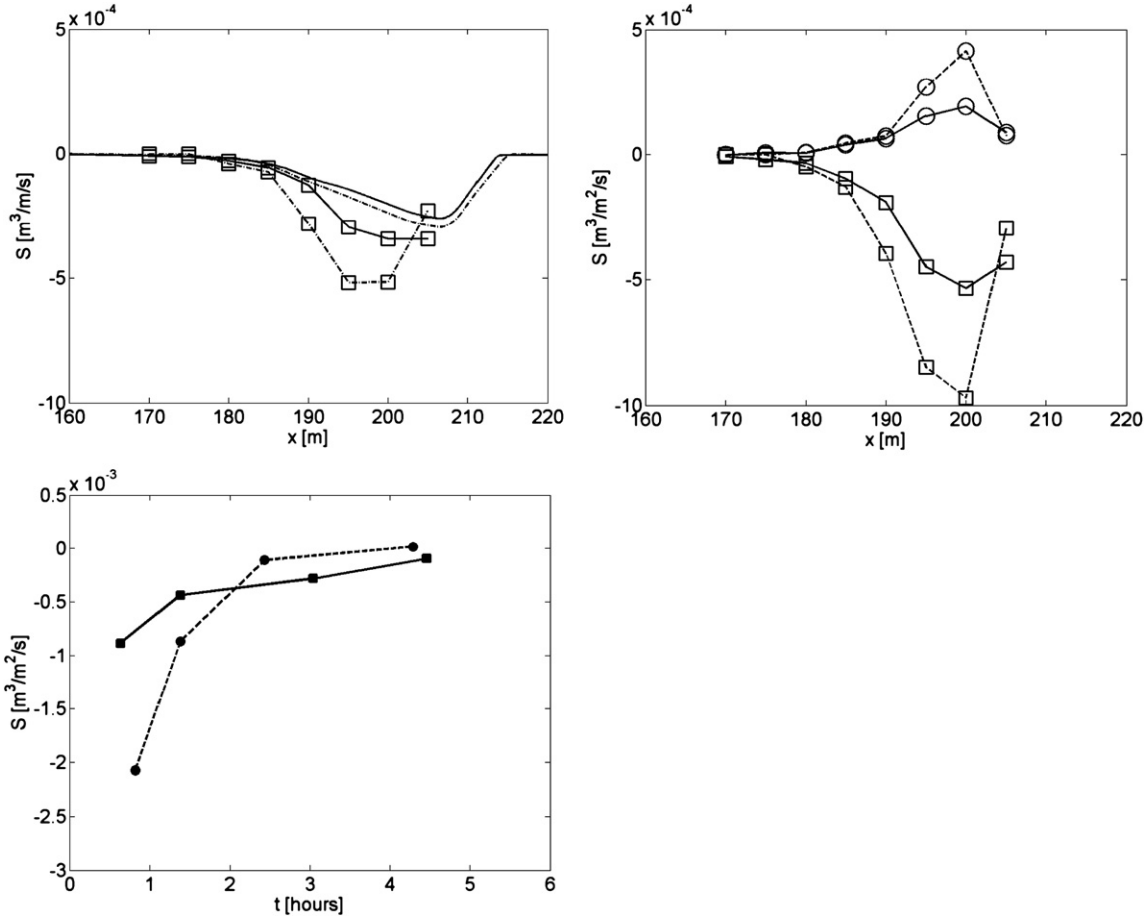

Fig. 9. Upper left panel: test averaged sediment transports as function of cross shore position for test T01 (solid line) and test T03 (dashed-dotted line). Lines with markers are transports computed from mobile frame measurements and the remaining lines are computed from bed level changes. Upper right panel: mobile frame sediment transports decomposed in the offshore mean flow related sediment transport (squares) and the onshore sediment transport ($S_{x2}+S_{x3}$) (circles) for test T01 (solid line) and T03 (dashed line). Lower left panel: temporal evolution of the total sediment transport measured with the mobile frame for test T01 (solid line) and test T03 (dashed line) at $x=200$ m.

x=200 m (Fig. 8, lower right panel) show that the total orbital velocities in test T03 are constantly about 15% larger. This is caused by an increase in long wave orbital flows whereas the short wave orbital velocities remain more or less the same.

Near-bed sediment concentrations during test T03 are O(100%) larger shore ward of x=185 m (Fig. 6, left panel). Evolution of sediment concentrations with progress of a test is comparable with test T01. Sediment concentrations decrease in time close to the dune face whereas further offshore concentrations increase (Fig. 6, right panel). Sediment concentrations during test T03 exceed that of test T01 during the whole experiment.

Comparison of test averaged sediment transport based on bed level changes show that the maximum sediment transports during test T03 is about 14% larger after 6 h (Fig. 9, upper left panel). Test averaged sediment transports computed from flow and sediment concentration measurements also show a larger sediment transport for increasing wave period, however this increase is larger as the 14% that was obtained for the profile evolution. In addition the maxima in the sediment transports, computed from flow- and sediment concentration measurements, are located further offshore.

Decomposing again the sediment transports from flow- and sediment concentration measurements into S_{x1}, S_{x2} and S_{x3} reveals that the increase in the maximum sediment transport is caused by an increase in the offshore directed flow related sediment transport. This rise is only partly compensated by an increase in the shore directed wave related transports and transports above the wave trough (Fig. 9, upper right panel). In addition Fig. 9, lower panel shows that the extra dune erosion due to a larger wave period occurs mainly at the start of the test whereas after approximately 2 h sediment transports in test T03 are smaller as during test T01.

5. Discussion/interpretation

It was found that the offshore directed time-averaged sediment transport is most important in predicting dune erosion. In addition it has been observed that an increase in the wave period results in an increase of the time-averaged sediment transport and therefore more dune erosion. In this section the physical processes responsible for the time-averaged offshore sediment transport are dealt with first, followed by a discussion on the effect of the increased wave period on the time-averaged sediment transport. Given the fact that the time-averaged flows for tests T01 and T03 are comparable (Fig. 8, upper left panel) the O(100%) increase in the time-averaged sediment concentrations is the main focus.

5.1. Time-averaged sediment concentrations

Sediment suspension is usually explained by the flow drag exerted on the bed. In addition most sediment concentration models relate the amount of suspension to the near-bed (orbital) flows to the third power (Bailard, 1981; Van Rijn, 1984; Nielsen, 1992). However in our experiments we find that measured time-averaged sediment concentrations poorly correlate with flow drag (Fig. 10, left panel). This poor correlation occurs for both the total near-bed velocities and the root mean square near-bed orbital velocities. From this we conclude that in the presented data set it is likely that also other physical processes are important to sediment suspension.

The sediment concentration measurements are mainly obtained in the inner surf zone where predominantly breaking saw-tooth shaped waves are present. These bores might affect sediment suspension in two ways:

1. Steep wave fronts under saw-tooth shaped waves imply larger spatial pressure gradients and by that increase the forces on the bed material causing additional sediment suspension (Madsen, 1974). In literature this mechanism is usually discussed as acceleration skewness (Nielsen, 1992; Drake and Calantoni, 2001; Hoefel and Elgar, 2003) where it is assumed that spatial flow gradients are relatively small in relation to temporal flow gradients and the flow is driven by pressure gradients.
2. Fronts of bores are unstable. As a result turbulence is generated that propagates over the water surface (surface roller) and into the water column. Depending on intensity- and type of wave-breaking turbulent vortexes might be able to reach the bed and stir up sediment as suggested by (Roelvink and Stive, 1989; Steetzel, 1993; Puleo et al., 2000; Reniers et al., 2004a). Also increased turbulence intensity over water depth causes sediment to stay longer in suspension resulting in larger time-averaged sediment concentrations (Van Rijn, 1993).

In the present data set it is not possible to distinguish between these two processes since they both occur at the front of a wave. As a consequence, in the following we will examine the combined effect of pressure gradients and wave-breaking generated turbulence on near dune sediment concentrations. We will assume that the spatial steepness of the wave front ($\partial\eta / \partial x$) is (also) related to the intensity of wave breaking, which seems not unlikely from a physical point of view (Longuet-Higgins and Turner, 1974; Deigaard, 1993).

In the analysis we derive a characteristic wave for each mobile frame measurement. Next, the shape of this wave is related to the time

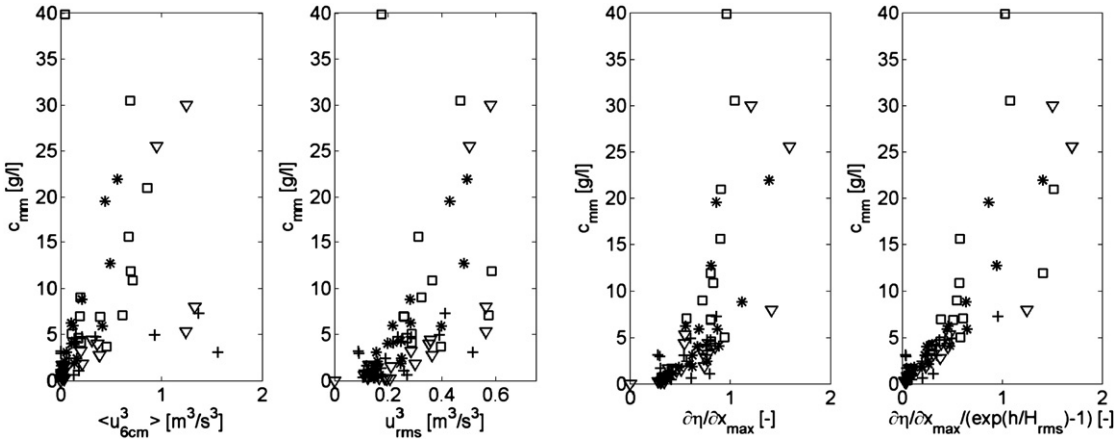

Fig. 10. Left panel: time and depth averaged sediment concentrations compared with respectively near-bed total flow velocity (correlation ρ=0.48) (left) and near-bed orbital flow (ρ=0.56) (right) for test T01 (asterisk), T03 (squares), T04 (pluses) and DP01 (triangles). Right panel: time and depth averaged sediment concentrations compared with the maximum wave surface slope (ρ=0.72) (left) and the maximum wave surface slope multiplied with an additional factor representing turbulence energy decay over depth (ρ=0.84) (right) for test T01 (asterisk), T03 (squares), T04 (pluses) and DP01 (triangles). The time and depth averaged sediment concentrations are obtained by vertical integration of suction tube measurements below mean water depth using a same procedure as proposed in Eq. (2).

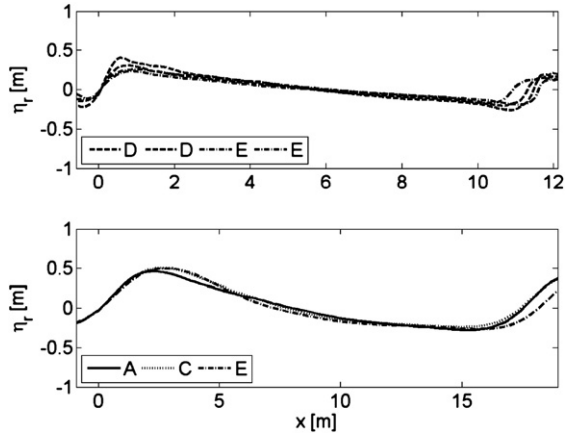

Fig. 11. Rescaled water surface elevations associated with a characteristic wave shape for test T01 at x=200 m (upper) and x=170 m (lower). Legends indicate the interval in which a mobile frame measurement was obtained. Within a test interval multiple measurements can be conducted at the same location (see upper plot at x=200 m).

and depth averaged sediment concentration in that measurement. Water surface elevation time series are divided into zero crossing waves after which the waves are rescaled and weighted summed as follows:

$$\eta_r(x) = \left(\sum_{i=1}^{i=n_{waves}} \left(\frac{H_{z,i}^2}{\sum_{i=1}^{i=n_{waves}} H_{z,i}^2} \frac{\eta(t_{1,i}:t_{2,i})}{L_{z,i}} \right) \right) L_{z,m} \quad (6)$$

where $\eta_r(x)$ is the characteristic wave surface elevation in space and n_{waves} is the number of zero down-crossing waves in a time series. $H_{z,i}=\eta_{max,i}-\eta_{min,i}$ where $\eta_{max,i}$ and $\eta_{min,i}$ are respectively the maximum and minimum water surface elevation within a specific zero down-crossing wave surface elevation signal $\eta(t_{1,i}:t_{2,i})$, where $t_{1,i}$ and $t_{2,i}$ are the times of the two consecutive zero down-crossings. $L_{z,i}$ is the wave length of a zero crossing wave and $L_{z,m}$ is the weighted zero crossing wave length over a measurement. The wave lengths and the conversion from time to cross shore coordinate position is obtained assuming the wave celerity is constant over a zero crossing wave: $L_{z,i}=c_i T_{z,i}$ and $x(t_{1,i}:t_{2,i})=t(t_{1,i}:t_{2,i})c_i$ where $c_i=w_i / k_i$ in which w_i is the radian frequency and k_i is the wave number associated with a zero crossing wave. A similar procedure is applied on the flow velocity time series by replacing $\eta(t_1:t_2)$ by $u(t_1:t_2)$ and $H_{z,i}$ by $U_{z,i}=u_{max,i}-u_{min,i}$ where $u_{max,i}$ and $u_{min,i}$ are respectively the maximum and minimum flow velocity within a specific zero crossing wave.

The water surface elevations associated with the characteristic waves in test T01 are plotted in Fig. 11 for two locations. It is observed that the characteristic wave shape evolves from a mainly Stokes shaped wave at x=170 m towards a pitched forward shaped wave with a steep wave front at x=200 m. In order to examine the effect of a changing wave shape on near dune sediment concentrations, the maximum gradient $\partial\eta / \partial x$ in the characteristic wave shape from each mobile measurement location is related to the corresponding time and depth averaged sediment concentration. All available measurements from test T01, T03, DP01 and T04, having different boundary conditions (T_p, spectral shape, and initial profile), are included. Near dune sediment concentrations apparently correlate much better with the maximum wave surface slope than with flow drag (compare Fig. 10, left- and right panels), from which we conclude that spatial pressure gradients and/or wave-breaking generated turbulence are likely to be important to sediment suspension in front of the dune face.

The spatial steepness of the wave front is presumed to be related to wave-breaking generated turbulence at the water surface. However this turbulence still has to be advected from the water surface to the bed in order to affect sediment suspension. It is therefore more appropriate to relate the near-bed turbulence intensity (instead of turbulence intensity at the water surface) to the measured sediment concentrations. Roelvink and Stive (1989) used an exponential decay model with the depth length proportional to H_{rms} to estimate the time-averaged turbulence energy at the bed from turbulence at the water surface:

$$k_b = \frac{k}{\exp(h/H_{rms}) - 1} \quad (7)$$

where k_b is turbulence variance at the bed and k is the time-averaged turbulence variance at the water surface. Applying this decay model as an additional multiplication factor to $(\partial\eta / \partial x)_{max}$, the correlation with the sediment concentrations improves significant (Fig. 10, right panel). Also the relation intersects the origin of the coordinate system which means that in deeper water, $((\partial\eta / \partial x)_{max} \neq 0)$, the effect of the wave front steepness on the sediment concentration vanishes since potential turbulence at the water surface does not reach the bed.

Considering larger sediment concentrations (c_{mm}>10 g/l) the relation with $(\partial\eta / \partial x)_{max} / (\exp(h / H_{rms})-1)$ becomes more scattered. Data points in this range are relatively few and obtained just in front of the dune face (x=200 or x=205 m) at the start of an experiment (interval A or B). It is unclear what causes the scatter, however dune face erosion rates in the initial phase of a test are large and irregular due to the

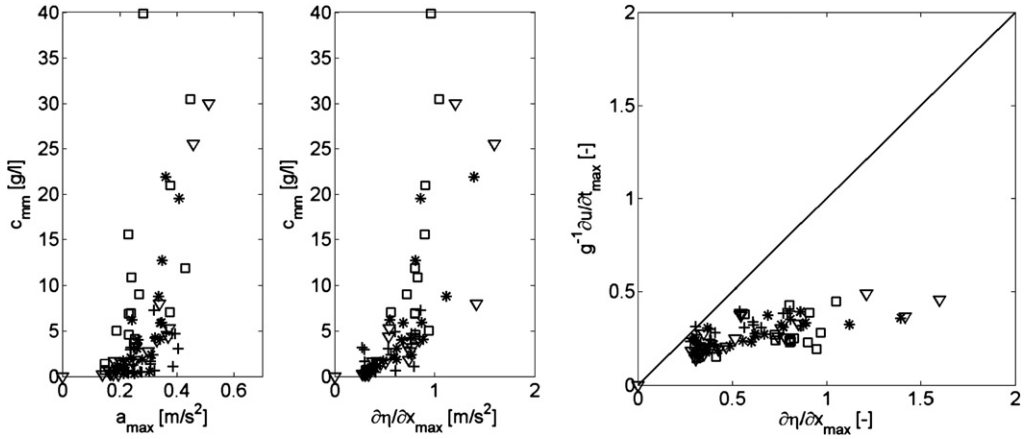

Fig. 12. Left panel: time and depth averaged sediment concentration compared with the maximum flow acceleration under the characteristic wave (left) and the maximum spatial steepness of this characteristic wave (right) for test T01 (asterisk), T03 (squares), T04 (pluses) and DP01 (triangles). Right panel: comparison of the maximum flow acceleration with the maximum wave surface slope for test T01 (asterisk), T03 (squares), T04 (pluses) and DP01 (triangles).

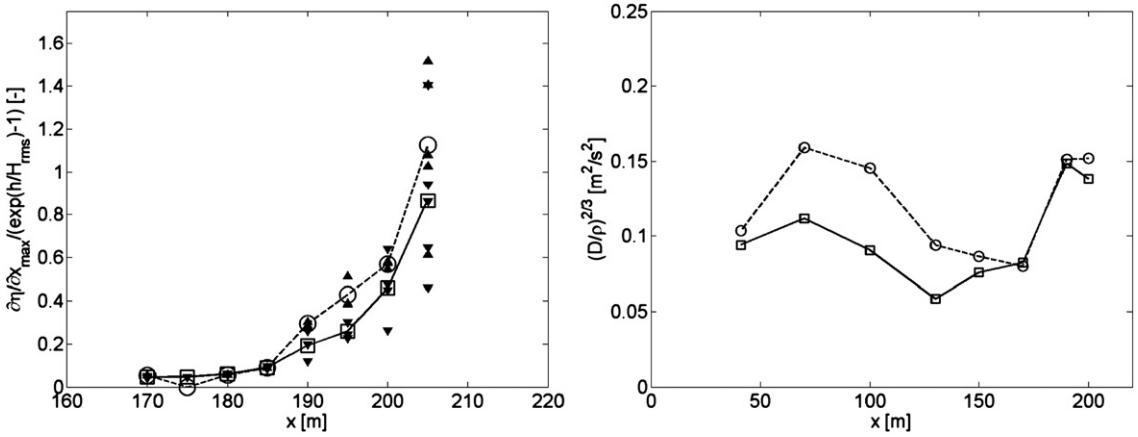

Fig. 13. Left panel: maximum wave steepness multiplied with an additional factor representing turbulence energy decay over depth as function of cross shore position for test T01 (solid line) and test T03 (dashed line). Open markers are the average of all mobile frame measurements at a location within a test. Right panel: test averaged wave energy dissipation as function of cross shore position for test T01 (solid line–squares) and test T03 (dashed line–circles).

episodically slumping of the dune face (Van Thiel de Vries et al., 2007; Van Gent et al., 2008) and might affect the sediment concentration just in front of the dune face, thereby masking the relation with the locally wave-breaking generated turbulence.

It is often assumed that under the assumption of $u\partial u / \partial x \ll \partial u / \partial t$ the local flow acceleration can be used as a proxy for the pressure gradient. However, the correlation of the time-averaged sediment concentrations in the inner surf with the maximum flow accelerations show considerably more scatter compared with the correlation with the maximum surface slope (compare results in Fig. 12, left panel). We found that the local flow acceleration accounts only for a part of the pressure gradient (Fig. 12, right panel). This is especially true close to the dune face where the waves are highly non-linear and spatially inhomogeneous.

5.2. Effect of the wave period on dune erosion

The measurements revealed that with increasing wave period the depth and time-averaged flows remain more or less the same whereas the time-averaged sediment concentrations increase with O(100%). As the large sediment concentrations in the near dune area have just been related to the spatial steepness of the wave front it seems logical to examine whether this steepness also clarifies the increase of the time-averaged sediment concentration with a larger wave period.

Indeed we find that for the larger wave period test, T03, the steepness of the wave fronts was on average larger (Fig. 13, left panel). Comparison with Fig. 6 reveals that the increase in the test averaged sediment concentrations as function of the cross shore position correlates well with the increase in wave steepness. We hypothesize that steeper maximum surface slopes during test T03 indicate more intensive wave breaking. As a result more turbulence is injected into the water column at the bore fronts and reaches the bed, increasing the suspension of sediment.

The latter is further examined by use of the pressure sensors spaced along the flume wall. A 4th order spline is fitted trough the energy flux Ec_g, where E is the measured wave energy (obtained from pressure measurements) and c_g is the wave group velocity associated with the $T_{m-1,0}$ wave period at the wave board computed from linear wave theory. Dissipation due to wave breaking is estimated as $D=\partial Ec_g/\partial x$ from which the turbulence variance k is computed as $(D/\rho)^{2/3}$ following Battjes (1975) (Fig. 13, right panel). It is shown that the test averaged energy dissipation due to wave breaking shoreward of $x=170$ m is comparable for both tests. Considering that the number of waves in test T03 is smaller, since waves in test T03 have a larger wave period, means that the amount of dissipation in a single bore has to be larger on average in test T03. This seems to be in line with our hypothesis that steeper maximum surface slopes during test T03 indicate a different, more intensive, type of wave breaking.

6. Conclusions

Large-scale dune erosion tests were conducted to obtain a better understanding of dune erosion physics. It was found that:

- Both long and short waves are important to near dune hydrodynamics. As a test continues and a new fore shore develops long waves become relatively more important.
- With progress of a test the amount of wave energy that reaches the dune face reduces with more than 30%.
- A partly standing wave pattern is observed near the dune face.
- Time and depth averaged flow velocities increase gradually with decreasing water depth till approximately −0.3 m/s and decrease with 25% near the dune face as the fore shore evolves.
- Time-averaged sediment concentrations 6 cm above the bed rise sharply towards the dune face from less than 1 g/l in deep water to more than 50 g/l. With progress of a test time-averaged sediment concentrations near the dune face decrease with more than 70%.
- Sediment transports decrease 95% with progress of a test and the maximum transport shifts shore ward with the retreated dune face. The flow related offshore directed sediment transport below the wave trough is dominant and is only partly compensated by the wave related sediment transport and sediment transports above the wave trough.

Further analysis of the time and depth averaged sediment concentrations revealed that these correlate much better with the maximum wave surface slope than with flow drag. This slope is associated with both the pressure gradient and wave breaking induced turbulence at the water surface. In order to obtain a measure for turbulence intensity near the bed, the maximum wave surface slope was multiplied with an exponential turbulence decay model from Roelvink and Stive (1989), which resulted in a significantly improved correlation with the time and depth averaged sediment concentrations. The pressure gradient was found to be only partly coupled to flow acceleration suggesting the latter should not always be used as a proxy for the first, especially in the near dune area with highly non-linear waves.

A 50% larger wave period during test T03 results in 24% more dune erosion after 2 h and 15% more erosion after 6 h (Van Gent et al., 2008). It was found that with a larger wave period:

- On average 10 to 15% more wave energy is observed near the dune face.

- Time and depth averaged flow velocities were found to be comparable and near dune orbital flow velocities increase with about 15%.
- Near dune sediment concentrations 6 cm above the bed increase with O(100%)
- The maximum time-averaged sediment transports during test T03 is about 14% larger after 6 h which is caused by an increase of the flow related, offshore directed sediment transport in the first hours of the test. This increase is only partly compensated by an increase of the wave related sediment transport and the sediment transport above the wave trough.

Further analysis revealed that the increase in dune erosion with a larger wave period is mainly caused by a rise in the time-averaged sediment concentrations O(100%). These larger sediment concentrations were explained by steeper maximum water surface slopes which are coupled to larger pressure gradients and an increase in wave-breaking generated turbulence. It was found that test averaged wave energy dissipation due to breaking is comparable for both tests with different wave periods. However this energy is dissipated by less waves in test T03 with a larger wave period, resulting in more intensive wave breaking and steeper wave fronts during this test.

Acknowledgements

This work was made possible by the funding of the Dr. Ir. Cornelis Lely Foundation, The Netherlands and the Delft Cluster Foundation, The Netherlands. We owe many thanks to the Delft Hydraulics staff at the Delta-flume facility for their technical support during the experiments. We thank Utrecht University, for bringing in their instruments and we thank RIKZ for providing funding for the experiments. We highly appreciate the constructive discussions with Prof. Dr. M.J.F. Stive and Dr. J van de Graaff as well as the discussions with Prof. Dr. L.C. van Rijn and T. van Maar on the mobile frame measurement setup. A.R. acknowledges funding through the Dutch National Science Foundation (NWO) contract DCB.5856.

References

Bailard, J.A., 1981. An energetics total load sediment transport model for a plane sloping beach. Journal of Geophysical Research 86, 10938–10954.
Battjes, J.A., 1975. Modelling of turbulence in the surfzone. Symposium on Modelling Techniques, San Francisco.
Bosman, J.J., Van der Velden, E.T.J.M., Hulsbergen, G.H., 1987. Sediment concentration measurements by transverse suction. Coastal Engineering 11, 353–370.
De Ronde, J.G., Van Marle, J.G.A., Roskam, A.P., Andorka Gal, J.H., 1995. Wave boundary conditions along the Dutch coast in relatively deep water (in Dutch). RIKZ-95.024. Institute for Coastal and Marine Management (RIKZ), The Hague, Netherlands.
Deigaard, R., 1993. A note on the three dimensional shear stress distribution in a surf zone. Coastal Engineering 20, 157–171.
Delft Hydraulics, 2006. Dune erosion: measurement report large scale model tests. Report No. H 4357. Delft Hydraulics, Delft, Netherlands.
Dette, H.H., 1986. Untersuchungen über Dünenabbrüche und stranderosion im grossen Wellenkanal. Die Küste (43), 247–282.
Dette, H.H., Larson, M., Murphy, J., Newe, J., Peters, K., Reniers, A., Steetzel, H., 2002. Application of prototype flume tests for beach nourishment assessment. Coastal Engineering 47 (2), 137–177.
Drake, T.G., Calantoni, J., 2001. Discrete particle model for sheet flow sediment transport in the nearshore. Journal of Geophysical Research 106 (C9), 19859–19868.
Fredsoe, J., Deigaard, R., 1992. Mechanics of coastal sediment transport. Advanced Series on Ocean Engineering 3.
Guza, R.T., Thornton, E.B., Holman, R.A., 1984. Swash on steep and shallow beaches. 19th International Conference on Coastal Engineering, Hawaii, pp. 708–723.
Hoefel, F., Elgar, S., 2003. Wave-induced sediment transport and sandbar migration. Science 299, 1885–1887.
Kraus, N.C., Smith, K.M., 1994. Supertank laboratory data collection project: volumes I and II. Main text and appendices. Technical Report CERC-94-3. Coastal Engineering Reserach Center, U.S. Army Engineer Waterways Experiment Station, Vicksburg, MS.
Longuet-Higgins, M.S., Turner, J.S., 1974. An 'entraining plume' model of a spilling breaker. Journal of Fluid Mechanics 63, 1–20.
Madsen, O.S., 1974. The Stability of a Sand Bed Under the Action of Breaking Waves. 182, Ralph M. Parsons Laboratory for water resources and hydrodynamics.
Nielsen, P. (Ed.), 1992. Coastal Bottom Boundary Layers and Sediment Transport. Advanced Series on Ocean Engineering. World Scientific. 324 pp.
Puleo, J.A., Beach, R.A., Holman, R.A., Allen, J.S., 2000. Swash zone sediment suspension and transport and the importance of bore-generated turbulence. Journal of Geophysical Research 105 (C7), 17,021–17,044.
Reniers, A.J.H.M., Roelvink, J.A., Thornton, E., 2004a. Morphodynamic modeling of an embayed beach under wave group forcing. Journal of Geophysical Research 109.
Reniers, A.J.H.M., Thornton, E.B., Stanton, T.P., Roelvink, J.A., 2004b. Vertical flow structure during Sandy Duck: observations and modeling. Coastal Engineering 51 (3), 237–260.
Roelvink, J.A., Stive, M.J.F., 1989. Bar-generating cross-shore flow mechanisms on a beach. Journal of Geophysical Research 94, 4785–4800.
Roelvink, J.A., Reniers, A.J.H.M., 1995. LIP 11D delta flume experiments. Report No. H 2130. Delft Hydraulics, Delft, Netherlands.
Roskam, A.P., Hoekema, J., 1996. Boundary conditions for wave periods along the Dutch coast (in Dutch). RIKZ-96.019. Institute for Coastal and Marine Management (RIKZ), The Hague, Netherlands.
Steetzel, H.J., 1993. Cross-shore transport during storm surges. Ph.D. Thesis, Delft University of Technology, Delft, Netherlands.
Van Gent, M.R.A., Van Thiel de Vries, J.S.M., Coeveld, E.M, De Vroeg, J.H., Van de Graaff, J., 2008. Large-scale dune erosion tests to study the effect of wave periods. Coastal Engineering 55, 1041–1051. doi:10.1016/j.coastaleng.2008.04.003.
Van Rijn, L.C., 1984. Sediment transport, Part II: suspended load transport. Journal of Hydraulic Engineering 110 (11).
Van Rijn, L.C., 1993. Principles of Sediment Transport in Rivers, Estuaries and Coastal Seas. Aqua Publications, Utrecht, The Netherlands.
Van Thiel de Vries, J.S.M., Clarke, L.B., Aarninkhof, S.G.J., Coeveld, E.M., Holman, R.A., Palmsten, M.L., Reniers, A.J.H.M., Stive, M.J.F., Uijttewaal, W.S.J., 2007. Interaction of dune face and swash zone. Coastal Sediments, New Orleans.
Vellinga, P., 1986. Beach and dune erosion during storm surges. Ph.D. Thesis, Delft University of Technology, Delft.